

Structural Order-Disorder Transitions and Phonon Conductivity of Partially Filled Skutterudites

Hyounghul Kim,¹ Massoud Kaviani,^{1,*} John C. Thomas,² Anton Van der Ven,² Ctirad Uher,³ and Baoling Huang⁴

¹Department of Mechanical Engineering, The University of Michigan, Ann Arbor, Michigan 48109, USA

²Department of Materials Science and Engineering, The University of Michigan, Ann Arbor, Michigan 48109, USA

³Department of Physics, The University of Michigan, Ann Arbor, Michigan 48109, USA

⁴Department of Mechanical Engineering, Hong Kong University of Science and Technology, Hong Kong, China
(Received 8 July 2010; revised manuscript received 20 September 2010; published 20 December 2010)

Filled skutterudites are high-performance thermoelectric materials and we show how their phonon conductivity is greatly influenced by the topology of the filler species. We predict (*ab initio*) the phase diagram of $\text{Ba}_x\text{Co}_4\text{Sb}_{12}$ and find several stable configurations of Ba ordering over the intrinsic voids. The phonon conductivity predicted using molecular dynamics shows a minimum in the two-phase mixture regime, dominated by significantly reduced long-range acoustic phonon transport.

DOI: 10.1103/PhysRevLett.105.265901

PACS numbers: 66.70.Df, 61.66.Dk, 63.20.dh, 64.75.Op

High-performance thermoelectric (TE) materials including skutterudites [1–4], metal silicides [5], complex chalcogenide compounds [6], clathrates [5,7], half-Heusler alloys [8], and oxides [9] are sought for efficient power generation. Skutterudites are particularly promising due to their robust mechanical properties [10] and allow for single or multiple filling with rare-earth and alkaline-earth metals that reduce the lattice thermal conductivity κ_L [1–4,11,12].

Binary skutterudites are compounds with the general formula MX_3 ($M = \text{Co, Rh, Ir}$ and $X = \text{P, As, Sb}$) having a crystal structure with a bcc lattice and belonging to the space group $Im\bar{3}m$. The structure consists of a periodic array of trigonally distorted and tilted MX_6 octahedrons. The metal M at the center is octahedrally coordinated by the pnictogen X [13]. The tilt of the MX_6 octahedrons gives rise to empty spaces (icosahedral voids) that form a body-centered sublattice. As first shown in [14], the voids are large enough and can be filled by foreign species entering as cations; however, the filler solubility limit is less than a full filling of all available voids [4,15].

Binary skutterudites possess very high charge carrier mobilities and the interest in these compounds as novel TE materials for power generation followed a suggestion [16] and observation [11] that their κ_L can be dramatically reduced upon filling the structural voids. Recent research has resulted in the TE figure of merit (ZT) of n -type skutterudites approaching the value of 1.5 at 800 K [17]. While the presence of the filler species in the skutterudite matrix seems to be essential for achieving low κ_L and hence high ZT , whether the filler acts as a rattling local vibration mode [1–4] or plays some other important role [7,18–20] remains controversial. So far the only insight into the role of ordered phases on the κ_L of partially-filled skutterudites has been the observation in [3] that the random distribution of filler ions scatter phonons more effectively than when most voids are filled. In this letter, we address the issue of ordering of the filler species, a topic

that has not yet been explored and that has a great influence on phonon scattering. To this end we examine $\text{Ba}_x\text{Co}_4\text{Sb}_{12}$, a skutterudite with a large filling fraction limit for Ba, using theoretical and computational treatments.

We begin with a determination of a temperature-composition phase diagram of $\text{Ba}_x\text{Co}_4\text{Sb}_{12}$ by combining *ab initio* calculations with the cluster expansion (CE) method and the Monte Carlo (MC) simulations. Thereafter, using equilibrium molecular dynamics (MD) simulations and the Green-Kubo fluctuation-dissipation linear response theory and κ_L decomposition, along with the phase diagram, we predict the κ_L of partially filled $\text{Ba}_x\text{Co}_4\text{Sb}_{12}$ as a function of concentration and temperature.

A prediction of phase stability at finite temperature requires the use of statistical mechanics to account for entropic contributions to the free energy. The most important source of entropy in a partially filled skutterudite arises from configurational degrees of freedom associated with all possible ways of distributing Ba and vacancies over the bcc sites of the filler sublattice. A mathematical description of these configurational degrees of freedom is possible with the CE method [21]. An occupation variable σ_i is specified for each Ba site i , which takes a value 1 if the site has a Ba atom occupant and -1 if it is vacant. The CE is constructed from this description, assuming an on-lattice Hamiltonian that can be expressed exactly as a series expansion of configurational basis functions of the form

$$E(\boldsymbol{\sigma}) = \sum_{\{\alpha\}} V_\alpha \Gamma_\alpha(\boldsymbol{\sigma}), \quad \Gamma_\alpha(\boldsymbol{\sigma}) = \prod_{i \in \alpha} \sigma_i, \quad (1)$$

where α denotes a cluster of Ba filler sites (pairs, triplets and so forth, as well as lone sites). All possible clusters of the sublattice sites are included in the sum. The $\Gamma_\alpha(\boldsymbol{\sigma})$ are cluster basis functions that form a complete and orthonormal basis within the Ba-vacancy configuration space [21]. The expansion coefficients V_α are referred to as effective cluster interactions (ECI) and can be determined from first principles. The CE describes the fully relaxed energy of the

crystal as a function of Ba-vacancy order or disorder and can be viewed as a generalized Ising model with physically realistic interaction parameters.

The series in Eq. (1) can be truncated to reflect the relatively small contribution from clusters comprised of many sites or those describing long-length scales. As a result, density-functional theory (DFT) total energy calculations can be used to parameterize the ECI and determine the truncation of the series. This was done using the DFT energies of 28 Ba-vacancy configurations over the filler sites of CoSb_3 [22]. The DFT calculations were performed using the Vienna *ab initio* simulation package [23] within the Perdew-Burke-Ernzerhof (PBE) parameterization of the generalized gradient approximation (GGA) for exchange and correlation [24] and using the projector augmented wave (PAW) method [25,26]. The optimized CE includes 10 ECI and has a cross validation score of 6 meV/site and a rms error of 4 meV/site.

By applying MC simulations to the cluster expanded Hamiltonian, it is possible to construct a temperature-composition phase diagram. The calculated phase diagram shown in Fig. 1(a) exhibits prominent ordered phases at Ba compositions below or near the experimental filling limit ($x \approx 0.44$) [27]; the γ phase has $x = 0.25$ and the α phase has $x = 0.5$. As shown in Figs. 1(b) and 1(c), the γ phase is highly anisotropic with Ba-Ba nearest neighbors (NN) along [111] and Ba-vacancy NN pairs along the other

$\langle 111 \rangle$ family axes; it disorders at $T_\gamma \approx 350$ K. Compared to that, the α phase has a higher symmetry with the filled Ba sites forming a diamond network; it disorders at $T_\alpha \approx 750$ K. Because all relevant phase transitions are first order, phase coexistence of the two phases can be obtained at intermediate x and low temperature. At higher temperatures coexistence of each phase with a solid solution is obtained.

The calculation of κ_L , and the interatomic potentials used in the MD simulations for the intermediate concentrations of Ba were based on the combinative rules (CRs) applied to the empty CoSb_3 and fully filled $\text{BaCo}_4\text{Sb}_{12}$ potentials from [20]. We use the Morse and three-cosine potentials, parameterized for two-body (Co-Sb, Co-Co, Sb-Sb, and Ba-Sb) and three-body (Co-Sb-Sb) interactions [20,22,28]. Interatomic potentials are simplified fields and the CRs are approximations, therefore these potentials cannot accurately predict, for example, formation energy. As related to κ_L , the structural parameters (Co-Sb first neighbor bond length r_o), elastic properties (bulk modulus E and elastic constant C_{ij}), average phonon speeds $u_{p,g,A}$, and specific heat capacity C_v (at 300 K) found from these potentials and from DFT are summarized in Table I. We compared the acoustic phonon characteristics, predicted using CRs and DFT, and found good agreement in their predicted phonon density of states and its integrated value (Fig. S3 in the supplement [22]). Using CRs, the prediction of κ_L at intermediate Ba composition is done with equilibrium MD and the Green-Kubo heat current (\mathbf{q}) autocorrelation function (HCACF) decay [20,30], i.e.,

$$\kappa_L = \frac{1}{k_B T^2 V} \int_0^\infty \langle \mathbf{q}(t) \mathbf{q}(0) \rangle dt, \quad \mathbf{q} = \frac{d}{dt} \sum_i E_i \mathbf{r}_i, \quad (2)$$

where k_B is the Boltzmann constant, V is the MD volume, T is the temperature, $\langle \mathbf{q}(t) \mathbf{q}(0) \rangle$ is the HCACF tensor, E_i is the energy of an atom (excluding the site energy), and \mathbf{r}_i is the atomic position vector. The details of the MD calculations are given in the supplementary material [22].

From Fig. 1(a), there are six qualitatively different structural configurations possible for Ba concentrations between $0 \leq x \leq 0.5$, at 300 K: three ordered ground-state structures ($x = 0, 0.25$, and 0.5), a solid solution ($0 < x \leq 0.16$), a mixture of γ phase and solid solution ($0.16 < x < 0.25$), and a two-phase mixture of ordered phases ($0.25 < x < 0.5$). Figure 2(a) shows the predicted κ_L of $\text{Ba}_x\text{Co}_4\text{Sb}_{12}$ as a function of Ba concentrations. As input configurations in the MD simulations, we used the ground-state ordered Ba configurations at $x = 0, 0.25$ and 0.5 , Ba solid solutions as obtained from MC snapshots ($x = 0.03$ and 0.14) and two-phase mixtures with a single interface (e.g., for $x = 0.38$ MD cell consisted of one half having the γ ordering at $x = 0.25$ and the other half having α ordering at $x = 0.5$; $x = 0.33, 0.38$, and 0.44). The results are in good agreement with experiment [27], showing that as the Ba concentration increases, κ_L decreases noticeably.

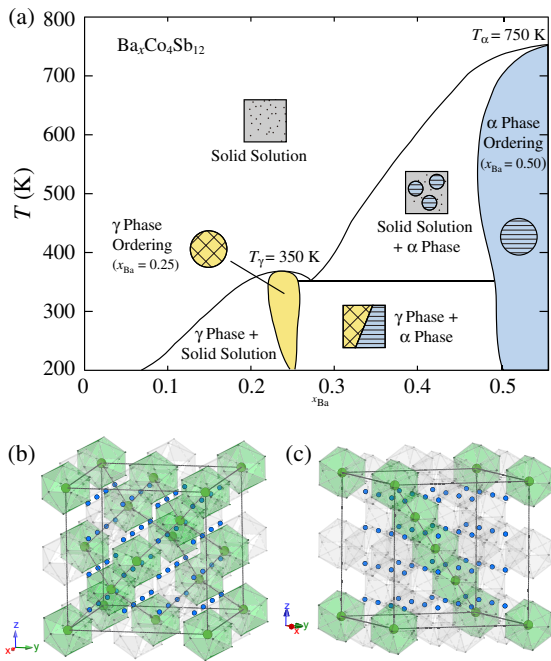


FIG. 1 (color online). (a) The solid-state phase diagram of $\text{Ba}_x\text{Co}_4\text{Sb}_{12}$ showing the order-disorder transition temperatures (T_α and T_γ). (b) Atomic structure of γ and (c) α phases. The Ba atoms (green circles) are shown in the ordered network structures. The Co atoms are shown with small blue circles. To avoid crowding, the Sb atoms at the polyhedron vertices are not shown.

TABLE I. Comparison of $\text{Ba}_{0.25}\text{Co}_4\text{Sb}_{12}$ properties obtained from CRs and DFT. The available results for CoSb_3 are also listed. The $u_{p,g,A}$ is along the Γ -N and Γ -H directions.

	r_o (Å)	E (GPa)	C_{11} (GPa)	C_{44} (GPa)	$u_{p,g,A}$ (m/s)	C_v (J/mol-K)
CRs	2.56	78	155	37	3098	22.9
DFT	2.54	82	126	54	2526	23.0
Literature	82 ^a	158 ^a	57 ^a	2934 ^b		

^afrom Reference [29].

^bfrom Reference [2].

The minimum conductivity relation κ_{\min} for the amorphous phase is also shown, and this gives $\kappa_{\min} \approx 0.37 \text{ W/m K}$ using CoSb_3 properties [22]. Starting with κ_L of CoSb_3 dominated by phonon-phonon scattering, we consider only phonon-point defects scattering and two-phase scattering for the compounds. On the top of Fig. 2(a), the state of the Ba-vacancy ordering and two-phase mixtures are marked. Since Ba more or less randomly fills the voids of CoSb_3 in the solid-solution regime, phonons propagate through the CoSb_3 host structure with the randomly distributed Ba atoms acting as point defects. As the phonon-boundary scattering is negligible except at low temperatures, this can persist up to $x = 0.25$ (fully ordered γ phase). The overall κ_L with the inclusion of phonon-point defects scattering is

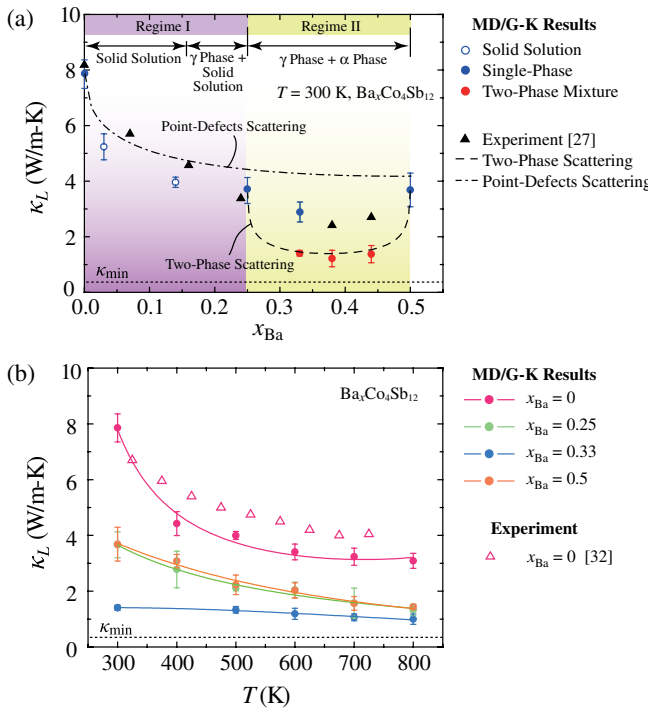


FIG. 2 (color online). Variation of predicted κ_L of $\text{Ba}_x\text{Co}_4\text{Sb}_{12}$. (a) Dependency on various Ba concentration at 300 K. The available experimental results [27], and the results of two analytical models [22] are also shown. (b) Temperature effects for several fill fractions. The available experimental results for CoSb_3 [32] are also shown. All error bars represent the standard errors.

$\kappa_L(x) = \kappa_L(0)/\{1 + c(x)[x(1-x)]^{1/2}\}$, where $c(x)$ is the coefficient for point-defects scattering with respect to x [22], and results are shown in Fig. 2(a), predicting significant phonon scattering in regime I. In the two-phase mixture ($0.25 < x < 0.5$), the mixture of two ordered phases (γ and α) creates significant interfacial scattering. This overall resistivity includes each phase resistivity ($1/\kappa_{L,\gamma}$ and $1/\kappa_{L,\alpha}$) and the interfacial resistivity ($1/\kappa_{L,d}$) simultaneously. While isolated point defects scatter phonons due to a point discontinuity in bonding and mass distribution, interfaces between two phases are two-dimensional discontinuities that scatter phonons. This interfacial resistivity had been previously treated the same as the point-defects scattering, so following that we use the treatment of [22], i.e., $1/\kappa_{L,d} = 0.888[x_{\gamma}(1-x_{\gamma})]^{1/2}(\text{m-K/W})$. We note that a more appropriate model would include the interface concentration and the impedance mismatch between the two phases as in the phonon-boundary resistance [31]. Then, we have $1/\kappa_L(\text{two-phase}) = x_{\gamma}/\kappa_{L,\gamma} + (1-x_{\gamma})/\kappa_{L,\alpha} + 1/\kappa_{L,d}$, where x_{γ} is the fraction of γ phase in a $\gamma - \alpha$ mixture. The dash line in Fig. 2(a) is for this two-phase scattering model and is in agreement with MD predictions. We note that it is the two-phase mixture causing the significant reduction in κ_L , by comparing with a hypothetical single-phase and the two-phase structures, for $x = 0.33$. The MD results for these structures are $\kappa_L(\text{single-phase, one of non-ground states}) = 2.9$ and $\kappa_L(\text{two-phase}) = 1.4 \text{ W/m-K}$ [data points and their uncertainties are given in the Fig. 2(a)]. The point-defects and two-phase scattering are two main reasons for the κ_L reduction in partially filled structures, compared with the empty structure. We also note that in the empty skutterudites the Umklapp scattering is important in the overall thermal conductivity as the point defects and two-phase scattering mechanisms are absent. In Fig. 2(a), the MD predicted $\kappa_L(\sim 1.0 \text{ W/m-K})$ and the two-phase scattering model show a minimum near $x = 0.38$, and this minimum is close to κ_{\min} , predicted for the amorphous-phase κ_L .

Figure 2(b) shows the predicted κ_L for $x = 0, 0.25, 0.33$, and 0.5, as a function of temperature, along with the experimental results [32]. The transition temperatures (T_{α} and T_{γ}) of two ordered phases are marked in Fig. 1(a), and at $T = 800 \text{ K}$ there is no ordered structure. So, we use the fully-disordered structures (configuration snapshots of the MC simulations). The single-phase crystal

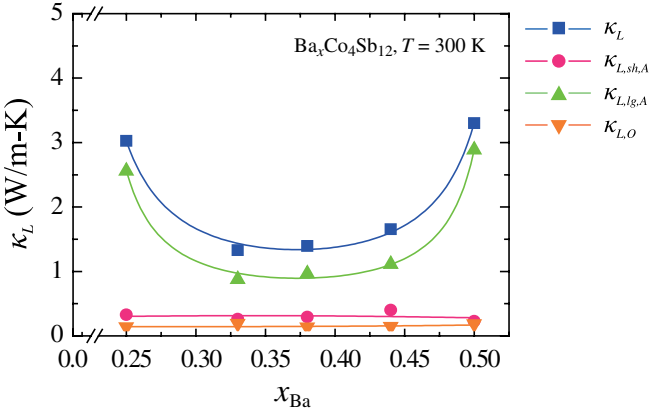


FIG. 3 (color online). κ_L decomposition and their variations with respect to Ba concentrations. Decompositions were done using singular MD simulation results for each concentration [as compared to Figs. 2(a) and 2(b) where average over several simulations was used].

follows the Slack relation ($\kappa_L \sim T^{-1}$ dependence for $T > 0.1T_D$) [33], while the two-phase mixtures reaches a plateau, similar to amorphous solid κ_{\min} [30]. This reconfirms that the two-phase mixtures can be considered as pseudoamorphous structures with significant reduction in κ_L for such crystalline TE materials.

In general, the heat is carried through skutterudites mostly by acoustic phonons, which are altered by the presence of fillers [7,18,20,27]. This significantly reduces κ_L for the two-phase mixtures and is also confirmed in an analysis of κ_L decomposition into the short-, long-range acoustic, and optical phonon components [30], i.e.,

$$\begin{aligned}\kappa_L &= \frac{1}{k_B VT^2} \left(A_{sh,A} \tau_{sh,A} + A_{lg,A} + \sum_i \frac{B_{i,O} \tau_{i,O}}{1 + \tau_{i,O}^2} \right) \\ &= \kappa_{L,sh,A} + \kappa_{L,lg,A} + \kappa_{L,O},\end{aligned}\quad (3)$$

where the τ_i denote time constants, A_i and B_i are constants, and the subscripts *sh*, *lg*, *A*, and *O* refer to short-range, long-range, acoustic, and optical. After removing the high-frequency components of HCACF with the Fourier low-pass filter ($f_{\text{cutoff}} = 1.5$ THz determined from phonon dispersion curves), the low-frequency acoustic portion are fitted with two exponential decay terms. Each component of HCACF in Eq. (3) was then integrated independently and Fig. 3 shows the results. The long-range acoustic phonon contribution is dominant and most affected by Ba concentrations, while the short-range acoustic and optical components are not. The $\kappa_{L,lg,A}$ decreases most noticeably by the two-phase scattering in the two-phase regime.

Our MD calculations indicate that in order to find a high-performance skutterudite-based TE materials, one can greatly benefit from the presence of order-disorder phase transitions of the filler species in the voids of the

skutterudite structure, which leads to two-phase coexistence and the presence of interfaces.

The work is supported by the Center for Solar and Thermal Energy Conversion funded by DOE, Office of Basic Energy Sciences (Grant DESC0000957).

*kaviany@umich.edu

- [1] B. C. Sales, D. Mandrus, and R. K. Williams, *Science* **272**, 1325 (1996).
- [2] G. P. Meisner *et al.*, *Phys. Rev. Lett.* **80**, 3551 (1998).
- [3] G. S. Nolas, J. L. Cohn, and G. A. Slack, *Phys. Rev. B* **58**, 164 (1998).
- [4] C. Uher, in *Semiconductors and Semimetals*, edited by T. Tritt (Academic, San Diego, 2000).
- [5] *Thermoelectrics Handbook: Macro to Nano*, edited by D. M. Rowe (CRC, Boca Raton, 2006).
- [6] K. F. Hsu *et al.*, *Science* **303**, 818 (2004).
- [7] M. Christensen *et al.*, *Nature Mater.* **7**, 811 (2008).
- [8] Y. Kimura and A. Zama, *Appl. Phys. Lett.* **89**, 172110 (2006).
- [9] I. Terasaki, Y. Sasago, and K. Uchinokura, *Phys. Rev. B* **56**, R12 685 (1997).
- [10] J. R. Salvador *et al.*, *Philos. Mag.* **89**, 1517 (2009).
- [11] D. T. Morelli and G. P. Meisner, *J. Appl. Phys.* **77**, 3777 (1995).
- [12] G. S. Nolas *et al.*, *J. Appl. Phys.* **79**, 4002 (1996).
- [13] S. Rundqvist and N. O. Ersson, *Arkiv. Kemi* **30**, 103 (1968).
- [14] W. Jeitschko and D. Brown, *Acta Crystallogr. Sect. B* **33**, 3401 (1977).
- [15] X. Shi *et al.*, *Phys. Rev. Lett.* **95**, 185503 (2005).
- [16] G. A. Slack, in *CRC Handbook of Thermoelectrics*, edited by D. M. Rowe (CRC, Boca Raton, 1995).
- [17] H. Li *et al.*, *Appl. Phys. Lett.* **94**, 102114 (2009).
- [18] M. M. Koza *et al.*, *Nature Mater.* **7**, 805 (2008).
- [19] D. Wee *et al.*, *Phys. Rev. B* **81**, 045204 (2010).
- [20] B. L. Huang and M. Kaviany, *Acta Mater.* **58**, 4516 (2010).
- [21] J. M. Sanchez, F. Ducastelle, and D. Gratias, *Physica (Amsterdam)* **128A**, 334 (1984).
- [22] See supplementary material at <http://link.aps.org/supplemental/10.1103/PhysRevLett.105.265901>.
- [23] G. Kresse and J. Furthmüller, *Phys. Rev. B* **54**, 11169 (1996).
- [24] J. P. Perdew, K. Burke, and M. Ernzerhof, *Phys. Rev. Lett.* **77**, 3865 (1996).
- [25] P. E. Blöchl, *Phys. Rev. B* **50**, 17953 (1994).
- [26] G. Kresse and D. Joubert, *Phys. Rev. B* **59**, 1758 (1999).
- [27] L. D. Chen *et al.*, *J. Appl. Phys.* **90**, 1864 (2001).
- [28] M. Marathe, M. Imam, and S. Narasimhan, *Phys. Rev. B* **79**, 085413 (2009).
- [29] L. Zhang *et al.*, *Mater. Sci. Eng. B* **170**, 26 (2010).
- [30] M. Kaviany, *Heat Transfer Physics* (Cambridge, New York, 2008).
- [31] S. Shin *et al.*, *Phys. Rev. B* **82**, 081302(R) (2010).
- [32] Y. Kawaharada *et al.*, *J. Alloys Compd.* **315**, 193 (2001).
- [33] G. A. Slack, in *Solid State Physics*, edited by F. Seitz, D. Turnbull, and H. Ehrenreich (Academic, New York, 1979)